Fine-structure contamination by internal waves in the Canary Basin

Louis Gostiaux[1] and Hans van Haren[2]

Received 26 March 2012; revised 17 September 2012; accepted 19 September 2012; published 3 November 2012.

[1] Over a range of 132.5 m, 54 temperature sensors (1 mK relative accuracy) were moored yearlong while sampling at 1 Hz around 1455 m in the open Canary Basin. Coherence between individual records shows a weak but significant peak above the local buoyancy frequency N for all vertical separations $\Delta z < 100$ m, including at sensor interval $\Delta z = 2.5$ m. Instead of a dominant zero-phase difference over the range of sensors, as observed for internal waves at frequencies $f < \sigma < N$, with f denoting the inertial frequency, this superbuoyant coherence shows π-phase difference. The transition from zero-phase difference, for internal waves, to π-phase difference is abrupt and increases in frequency for decreasing $\Delta z < 10$ m. For $\Delta z > 10$ m, the transition is fixed at $N_t \simeq 1.6N$, which is also the maximum value of the small-scale buoyancy frequency, and limits the internal wave band on its high-frequency side. In the time domain it is observed that this high-frequency coherence mainly occurs when nonlinearities in the temperature gradient, such as steps in the temperature profile, are advected past the sensors. A simple kinematic model of fine-structure contamination is proposed to reproduce this observation. The canonical -2 slope of the temperature spectrum above N is not observed in the in situ data, which rather slope as $-8/3$. The $-8/3$ slope can, however, be reproduced in our model, provided the jumps in the temperature profile are not infinitely thin.

Citation: Gostiaux, L., and H. van Haren (2012), Fine-structure contamination by internal waves in the Canary Basin, *J. Geophys. Res.*, *117*, C11003, doi:10.1029/2012JC008064.

1. Introduction

[2] The result of downward transport of heat in the ocean is an interior that is vertically stratified in potential density from surface to bottom. To first order, this is modeled with a smoothly increasing density profile, of which the gradient decreases with increasing depth. To second order, surface and bottom boundary layers are homogeneous, and the density gradient shows a maximum at a depth of 100–300 m in the seasonal pycnocline. To third order, the ocean interior density profile consists in many locations of a large number of steps, in which weakly and strongly stratified layers alternate varying in thickness O(1–100) m, but for which a scale of 10 m seems canonical. This scale is separating internal wave shear and turbulence [*Gargett et al.*, 1981], and below it the temperature gradient variance rolls off [*Gregg*, 1977].

[3] All these different density variations with depth can support internal waves. While linear waves do not transport material, nonlinear waves to the point of breaking can mix fluid and suspended material. Although the dominance of internal wave-induced mixing for open ocean transport is well accepted, the precise amount and mechanism are still under research. In that ongoing search for processes linking internal waves and mixing, understanding the transition between the internal wave band and the superbuoyant wave band is crucial. If there is wave induced turbulence, energy should be transferred to higher frequencies in this region. The amount of mixing needed to sustain the global advection-diffusion balance can be inferred from heat and salinity budgets in the ocean, but whether this mixing occurs in the open ocean [*Munk*, 1966] or mainly close to the boundaries [*Garrett*, 1990; *Munk and Wunsch*, 1998] is still an open question. A commonly proposed mechanism for internal wave-induced mixing is shear instability, whereby large-scale motions, more commonly low-frequency internal waves near the inertial frequency f, create vertical current shear upon which small-scale high-frequency internal waves become deformed and eventually break [e.g., *Phillips*, 1977]. Such mechanism was recently highlighted using fast and accurate temperature measurements above Great Meteor Seamount [*van Haren and Gostiaux*, 2010], but observations of internal wave breaking in the open ocean are still very rare [*Alford and Pinkel*, 2000; *Thorpe*, 2010].

[4] Finding some evidence of this wave-turbulence transition was one of the objectives of the Long-term Ocean Current Observations (LOCO) program in the Madeira-Canary Basin;

[1]Laboratoire de Mécanique des Fluides et d'Acoustique, UMR 5509, CNRS, École Centrale de Lyon, Université de Lyon, Ecully, France.
[2]Royal Netherlands Institute for Sea Research, Den Burg, Netherlands.

Corresponding author: L. Gostiaux, Laboratoire de Mécanique des Fluides et d'Acoustique, UMR 5509, École Centrale de Lyon, Université de Lyon, 36 ave. Guy de Collongue, FR-69134 Écully CEDEX, France. (louis.gostiaux@ec-lyon.fr)

0148-0227/12/2012JC008064

the LOCO11-3 mooring and its thermistor string data, on which the present article will now focus, reveal however that fine-structure contamination partially overrides the signal in the superbuoyant wave band.

[5] Fine structure has been studied since the development of CTD and microstructure profilers allowed to resolve the vertical scales of temperature and salinity in the ocean [*Osborn and Cox*, 1972; *Gregg and Cox*, 1972]. In the context of internal waves, it rapidly appeared that the advection of oceanic fine structure may lead to erroneous interpretations of temperature measurements, and much theoretical work was performed to distinguish real internal wave signal from so-called "fine-structure contamination." The pioneering work of *Phillips* [1971] revealed that the vertical advection of temperature steps by internal waves contaminates temperature records at fixed depths. Fine-structure contamination can be recognized in the superbuoyant part of temperature spectrum as a typical -2 slope with frequency, theoretically predicted for sharp staircases in the temperature profile. *McKean* [1974] developed this theory using the formalism of *Garrett and Munk* [1971]. He quantified the effect of fine-structure contamination on temperature and vertical coherence spectra in the internal wave band. This method is successfully used by *Joyce and Desaubies* [1977] using data from the IWEX experiment. The interest for fine-structure contamination decreased thereafter, because the layering was more considered to be a transient feature of the flow, which is probably true in highly energetic regions like the thermocline, but less obvious in the deep ocean. In any case, measurements of the effects of fine-structure contamination on superbuoyant coherence and comparison with analytical models are still missing. Newly designed temperature sensors used by the present study allow to resolve this process in detail.

2. Data and Background

[6] In order to learn more about small- and large-scale open-ocean internal wave motions, we taped 54 NIOZ High Sampling Rate Thermistors (NIOZ HST version 3) sensors to a steel mooring cable at 2.5 m intervals [*van Haren et al.*, 2009]. This thermistor string was mounted 10 m below the elliptical top buoy of a 3875 m long mooring at 33°00.010′N, 22°04.841′W, H = 5274 m water depth to the west of Madeira, NE Atlantic Ocean between May 2006 and November 2007. The sensors sampled at a rate of 1 Hz to a relative accuracy better than 0.001°C. For details of the mooring, see *van Haren and Gostiaux* [2009]. As a result of the large net buoyancy, low-frequency (subinertial) mooring motion due to current drag varied less than 1.2 m vertically and did not substantially affect the temperature observations. In the present study, we restrict ourselves to the first 200 days of data, ranging between year days 162 to 362, 2006. In doing so, we stay away from the influence of a strong meddy passing on our mooring in February 2007, and we also maximize the number of sensors properly working (53 out of 54). This number started to decrease in 2007 as some sensors ran out of battery. A downward looking 75 kHz ADCP in the top buoy provided velocity data over the range of measurement of the thermistor string (and deeper) every 30 min.

[7] Prior to and after the deployment period, 24 Hz sampled CTD profiles were obtained to calibrate NIOZ HST sensors and to establish local N, which is thus poorly resolved in time but well resolved in the vertical. The precise $N(z)$ depends on its vertical length scale Δz in association with a duration of time that should be larger than the particular internal wave of interest, as internal waves deform the stratification at rest. N could not be computed from temperature data alone, as inversions were observed regularly due to Mediterranean outflow influence. Here we compromise and compute an N_s distribution using arbitrary short-scale $\Delta z_s = 1$ m (which is the shortest scale over which N is realistically computable using CTD data stacked in 0.33 m vertical depth bins), an N_m distribution using moderate scale $\Delta z_m = 10$ m and a large-scale N_l value approximately across the range of the thermistors using $\Delta z_l = 100$ m. As shown in *van Haren and Gostiaux* [2009], $N_l = \bar{N}_m = \bar{N}_s = 26$ cycles per day (cpd), is used as a canonical value of N for large (vertical) scale internal waves, the overbar denoting an averaging. We also define a transition buoyancy frequency which limits the internal wave band on its high-frequency side, $N_t \simeq \max(N_m)(\Delta z_m = 10\ \text{m}) \simeq 42$ cpd, as far as can be established from the limited CTD data over the range of the thermistors.

3. Observations

[8] Space-time series of temperature along the thermistor string range reveal coherent vertical motions of the isotherms over $f < \sigma < N$, which is evidence of internal wave activity far away from any topography. Figure 1a shows two days of temperature record. Each of the 53 temperature sensors are displayed independently using the same color scale; continuity along the vertical is thus a manifestation of the precision of the NIOZ HST thermistor string. Homogeneous layers of typically 60 m thickness, visible in the temperature profiles of Figure 1b, are present all along the record, and persistent over several days [*van Haren and Gostiaux*, 2009]. As the temperature is measured using moored sensors, horizontal advection by mean flows is probably responsible for this low-frequency variability because these layers have finite horizontal extensions. This means that the effective time persistency of the may be longer than 10 days. Such layers are commonly observed in the Mediterranean outflow [*Magnell*, 1976], and are possibly created by double diffusion [*Merryfield*, 2000]. In the rest of the article, we will focus on high-frequency, vertical advection of such layers by internal waves.

[9] The mean vertical velocity is computed by maximizing the correlation between two successive temperature profiles separated by $\delta t = 30$ s, after introducing a vertical shift δz. The elevation curve plotted in Figure 1 is the time integral of this vertical shift $\zeta(t) = \int \delta z(\tau) d\tau$. The technique of vertical velocity extraction from temperature data was proposed by *Pinkel* [1981]. It was then applied to temperature time series in the thermocline, where the persistency of the layers is shorter than in the present data set, most probably because of a higher level of turbulence. Our improvement is that we compute correlations instead of directly tracking isotherms, which allows for extraction of the vertical velocity signal over the complete data set, without restricting ourselves to regions where isotherms are distinctly identifiable within the range of sensors. In our case, the elevation signal is computed using the entire vertical range of temperature sensors (132.5 m) and

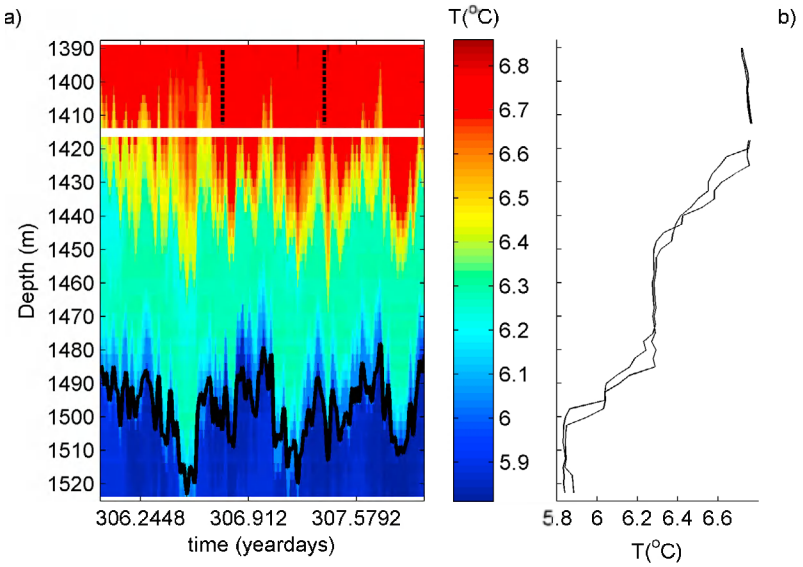

Figure 1. (a) Two days of temperature data collected by the NIOZ HST string, unfiltered. Superimposed is the elevation signal $\zeta(t)$ (thick black line) computed from the average vertical displacement over the whole vertical range of thermistors. This curve, which could be plotted at any depth (by vertical translation), here arbitrarily starts at 1485 m. (b) Two instantaneous temperature profiles separated by 20 h, showing a persistent homogeneous layer of 60 m thickness. The dates corresponding to the two profiles are marked by two dashed lines in Figure 1a.

thus corresponds to (local) mode 1 displacements over this range. This does not imply anything on the global vertical structure of the internal tide over the entire water column. Our choice is motivated by the absence of local higher modes motions in the data (see Figure 1, which is representative of the whole data set) and is further validated in the article.

[10] The computed vertical velocity signal $\zeta_t = d\zeta/dt$ is comparable in amplitude with the ADCP vertical velocity signal averaged over the range of the thermistor string, but is less noisy and better resolved in time. Figure 2a shows the velocity spectra inferred from the ADCP between days 162–362 superimposed on the vertical velocity spectrum inferred from the isotherms displacements. The latter vertical velocity signal has a noise level that is one order of magnitude lower than that of the ADCP, and it is not affected by the diurnal plankton motions. These motions, in phase with the sun and top hat in shape, create a series of peaks (S_1, S_2, S_3, etc.) in the vertical velocity spectrum from the ADCP. Near-buoyancy frequency motions are also better resolved by the isotherm displacement, as the velocity is estimated over $\delta t = 30s \ll 2\pi/N$, whereas the ADCP sampling rate was 30 min. The slopes of the internal wave band continuum, -1 and $+1$ for horizontal and vertical velocities respectively, differ from GM72 theory [*Garrett and Munk*, 1972], for which -2 and 0 slopes are expected, but are in good agreement with the internal wave dispersion relation:

$$\tan^2\theta = \frac{\omega^2 - f^2}{N^2 - \omega^2}.$$

[11] This relation gives the angle θ of propagation of the waves and thus a measure of the ratio between horizontal and vertical kinetic energy in a vertical plane aligned with the direction of propagation of the waves. In our case, the velocities measured using the ADCP are projected on fixed directions in a Cartesian frame of reference, whereas internal waves may have any azimuthal angles associated with their generation point. For an isotropic wave field, the ratio between vertical and horizontal kinetic energy is equal to $r = E_v/E_h = \tan^2\theta/(1 + f/\omega)^2$, f/ω being the ratio between along-wave and cross-wave horizontal velocity, also interpreted as the aspect ratio of the horizontal hodograph [*Pinkel et al.*, 1987].

[12] This energy ratio is computed using horizontal velocities from the ADCP data and using vertical velocities from the isotherm displacements inferred from the thermistor string data (Figure 2a, thick line). The agreement with theory is very good in the range $[f;\sigma_1]$, where $\sigma_1 = \sqrt{(N^2 - f^2)/2}$ is the frequency at which horizontal and vertical kinetic energy should be equal. For $\sigma > \sigma_1$, at which motions get more vertical, the horizontal currents are reaching the noise level as the spectrum becomes white, whereas vertical velocity measurements using the temperature data are still reliable. This is the reason for the underestimate of the ratio E_v/E_h as σ gets closer to N. When the ADCP data are used to estimate the vertical velocity (Figure 2a, thin dashed line), peaks due to plankton migration appear, and agreement at high frequencies is less good.

[13] The consistency with the dispersion relation proves the quality of the present spectra. However, it does not match the canonical slopes from *Garrett and Munk* [1972]. The exponents used by the GM72 model were inferred from observations, not from theory. If many measurements match with these so-called "universal" exponents, some exceptions exist. *Ferrari and Wunsch* [2009, Figure 2] provide an example of internal wave energy spectra that do not match GM72 [*Fu et al.*, 1982]. In Figure 3 of *Pinkel* [1981], the vertical velocity spectrum, inferred from isotherm

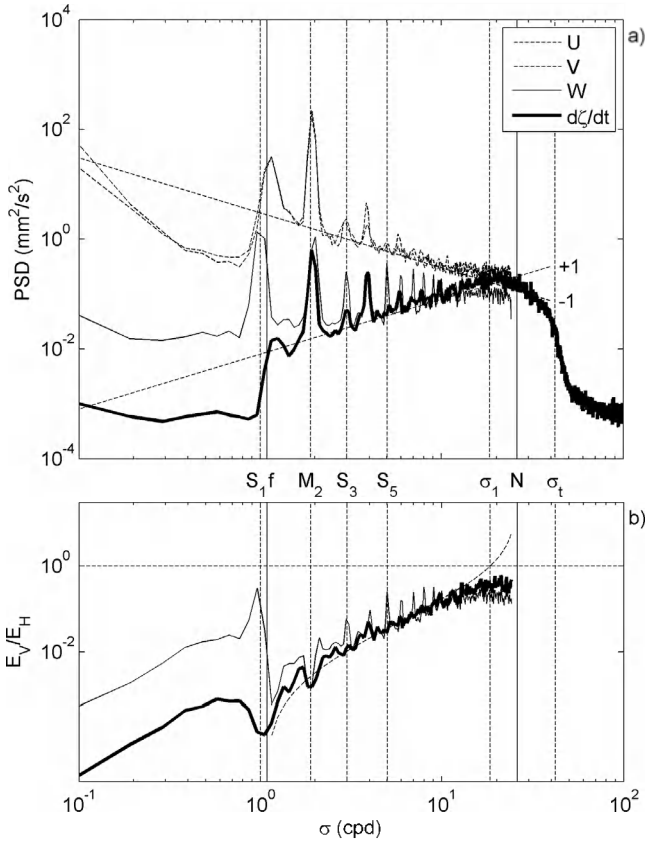

Figure 2. (a) Velocity spectra from the ADCP (thin lines), with U, V, and W for east, north and vertical (upward) velocities. The thick line graph indicates the vertical velocity spectrum from the time derivative of the elevation signal $\zeta(t)$. Spectra are computed over 200 days of data starting year day 162, 2006. ADCP data are sampled every 30 min, while the elevation $\zeta(t)$ is computed every 15 s. (b) Ratio between the vertical and horizontal kinetic energy, using for the vertical velocity either the ADCP data (thin line) or the derivative of $\zeta(t)$ resampled every 30 min (thick line). The theoretical prediction from the dispersion relation is given by the dashed line. Vertical thin dashed lines indicate relevant tidal constituents and typical frequencies defined in the text.

displacements, has a +1 slope at high frequency, though more coarsely resolved than in the present data set and not discussed by the author.

[14] The dominance of internal waves in the *f*-*N* band suggests that temperature signals recorded by individual thermistors at different levels should be highly coherent in this range of frequencies. Indeed, the interior Madeira-Canary Basin (200 days) mean temperature coherence spectra computed over small vertical scales are dominated by a significant weakly sloping plateau that roughly ranges from near-inertial frequencies to the large-scale buoyancy frequency N (Figure 3a). At larger vertical separation between the sensors, coherence rapidly decreases, although still being statistically significant, with largest coherence at semidiurnal frequencies. However, it appears that the coherence increases for values of $\Delta z \simeq \bar{D} =$ 60 m (Figure 3a, black line) before diminishing again for $\Delta z \simeq$ 100 m. This specific vertical scale $\bar{D}$ happens to be the typical thickness of weakly stratified layers, and this indicates a strong relationship between these coherency data and the background thermal structure. The characterization of $\bar{D}$ is given in Appendix A.

[15] In terms of frequency, the internal wave band coherence clearly shrinks in frequency range with increasing vertical separation until $\Delta z = 10$ m. Within the internal wave band $f < \sigma < N$ mean phase difference is 0, and vertical mode 1 waves dominate for all particular Δz (Figures 3b–3g). The present data clearly demonstrate an abrupt change in phase differences at frequencies higher than the buoyancy frequency. At particular σ, the spectrum shows a significant π-phase difference ($170 \pm 12°$ for $\Delta z = 5$ m, and similar mean values but larger errors for larger vertical distances). Such observation have been reported for the coherence between temperature difference time series from the IWEX data set [see *Joyce and Desaubies*, 1977, Figure 9]. Temperature difference is more

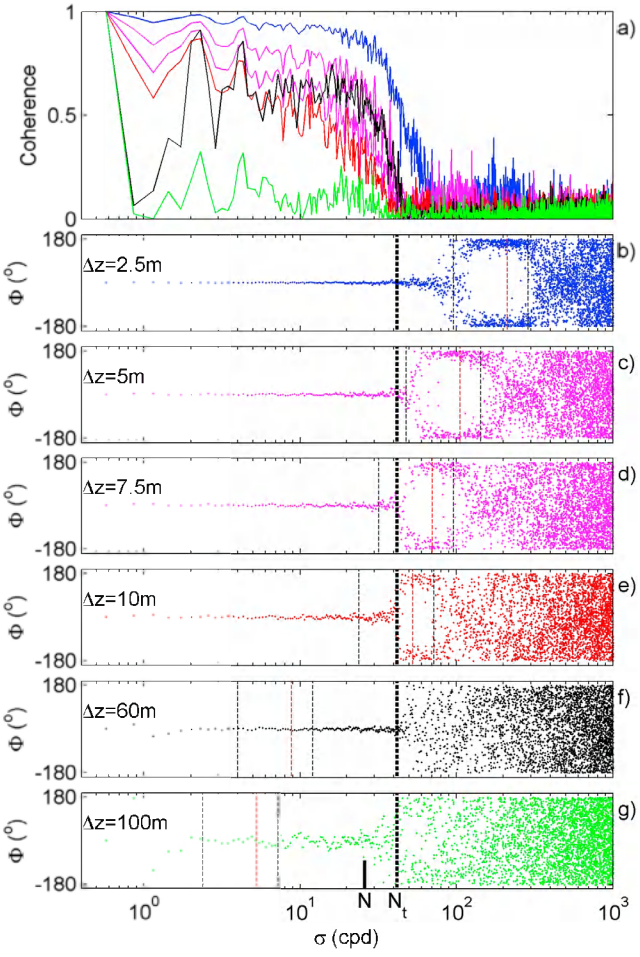

Figure 3. Coherence spectra between thermistors separated by Δz in the vertical. Spectra are computed over 200 days of in situ data. (a) The absolute value of coherence for $\Delta z =$ 2.5 m (blue line), 5 m (magenta line), 7.5 m (magenta line), 10 m (red line), 60 m (black line), and 100 m (green line). The 95% significance level is at coherence = 0.1. (b–g) Phase with corresponding colors. The thick dashed line represents N_t, the transition frequency, whereas thin dashed black and red lines correspond to our theoretical model for the π-phase region, which is described in section 4.

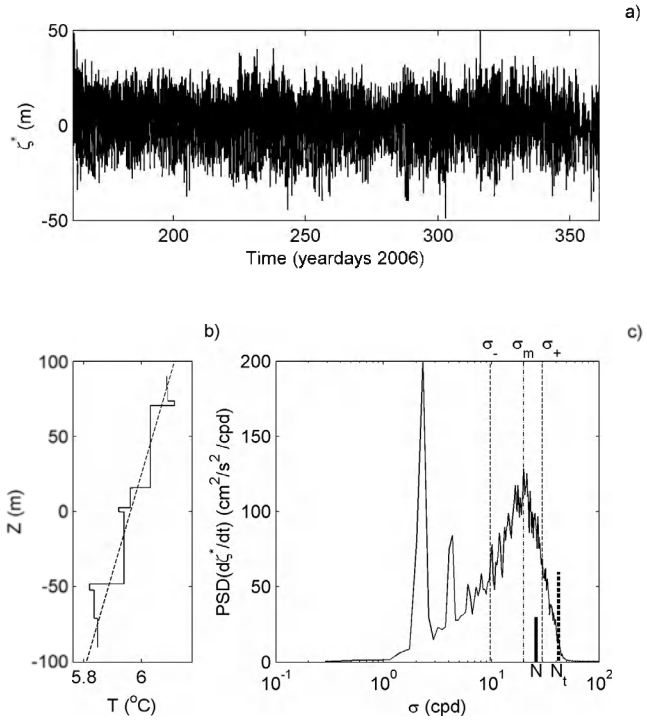

Figure 4. (a) High-pass-filtered elevation signal ζ^* that is used to advect (b) the artificial temperature profile. This profile consists of 10 temperature steps of uniformly random amplitude between −0.2 and 0.8°C. The locations of the steps in the vertical are also uniformly random. (c) The spectrum of the vertical velocity $d\zeta^*/dt$ in lin-log, which is used to compute the range of the high-frequency internal wave band. Here σ_- and σ_+ (dashed lines) define the width of the maximal vertical velocity peak around σ_m (dash-dotted line). N and N_t are also indicated.

sensitive to fine-structure contamination, more especially inside the internal wave band. But the other reason for which observations of π-phase difference between vertically separated sensors have never been shown for temperature is that this difference occurs at high (superbuoyant) frequencies, which were not resolved using classic low-frequency instrumentation. Our high sampling rate temperature sensors allow us to observe this phenomenon.

[16] As far as can be established, the π-phase difference band has a fixed length in log space for $\Delta z < 10$ m. For increasing $\Delta z > 10$ m, a blockade appears precisely at $N_t > N$, the maximum small-scale (10 m) buoyancy frequency, resulting in a shrinking of the π-phase region. At even higher frequencies, higher than the π-phase region, the phase differences seem to resume a mean around 0, before adopting random distribution. Coming from low, internal wave frequencies, the transition from 0 to π-phase difference is very abrupt, and associated with N_t for $10 < \Delta z < 100$ m. It is more gradual for $2.5 < \Delta z < 10$ m, for which the π-phase difference is reached at frequencies increasing for decreasing Δz.

4. Interpretation

[17] A simple kinematic model is used to reproduce the coherence spectra of Figure 3. The observed mean elevation signal of the isotherms is used to advect an artificial, time-independent temperature profile passed a virtual thermistor chain. For computational reasons, the elevation signal $\zeta(t)$ is high-pass filtered above 0.5 cpd, in order to avoid the isotherms to run out of the interpolation region. The filtered signal ζ^* has a standard deviation of 11.5 m (Figure 4a). The temperature profile used in Figure 4b consists of 10 infinitely thin temperature steps. Their amplitude is uniformly random between −0.2 and 0.8°C (thus allowing inversions as observed in the in situ data) and their locations in the vertical is also uniformly randomly distributed over a range of 200 m. To this profile, a mean temperature $T_0 = 6$°C is added, the value of which has no effect on the following results. A set of 20 random profiles have been generated, all leading to the same conclusions, but for clarity we choose to present results for a single realization.

[18] The advection of an infinitely thin temperature step passed a sensor recording temperature at depth z_n will generate a top hat signal which is described by the convolution of the elevation signal with a Heaviside function H. If Z_k is the depth of the temperature step in the profile at rest, and T_k the temperature above step number k we have

$$T(z_n, t) = T_0 + \sum_{k=1}^{n_{steps}} T_k H(Z_k + \zeta^*(t) - z_n). \quad (1)$$

[19] Doing so, we assume that our artificial temperature profile does not change with time over the total duration of our elevation signal (200 days), which is not realistic. However, as will be shown, this very simple model is able to correctly reproduce the observations of Figure 3, which indicates that slow temporal variations of the temperature profile do not play a significant role in the fine-structure contamination phenomenon.

[20] The temperature signal in equation (1) is a succession of staircases, positive and negative, occurring every time a temperature jump passes the sensor (Figures 5b–5d). Two sensors nearby in the vertical will record very similar signals, yet slightly shifted in time. An upgoing motion of a wave will affect the lowest thermistor with a slight advance, while a downgoing motion of a wave will affect the lowest thermistor with a slight delay. As a result, the difference between the temperature signals of the two sensors is nonzero, but consists of spikes occurring every time a temperature step passes the two sensors successively (Figures 5e and 5f). The duration Δt of these spikes increases linearly with the vertical spacing between the two sensors Δz. It can roughly be estimated by the formula $\Delta t = \Delta z/\bar{w}$, $\bar{w}$ being the typical vertical velocity of the advected temperature step. Similar scaling is found in *Garrett and Munk* [1971]. These spikes correspond to a π-phase coherency between the two thermistors separated by Δz, provided there is no other dominant signal superimposed on this fine-structure contamination. This can only occur for the superbuoyant frequency range as the internal wave band is dominated by coherent vertical motions. We thus have to estimate $\bar{w}$ in the near-N band.

[21] The variance of the vertical velocity (Figure 4c) could be used for that purpose. However, as the near-N motions are intermittent, broadband and not deterministic, the

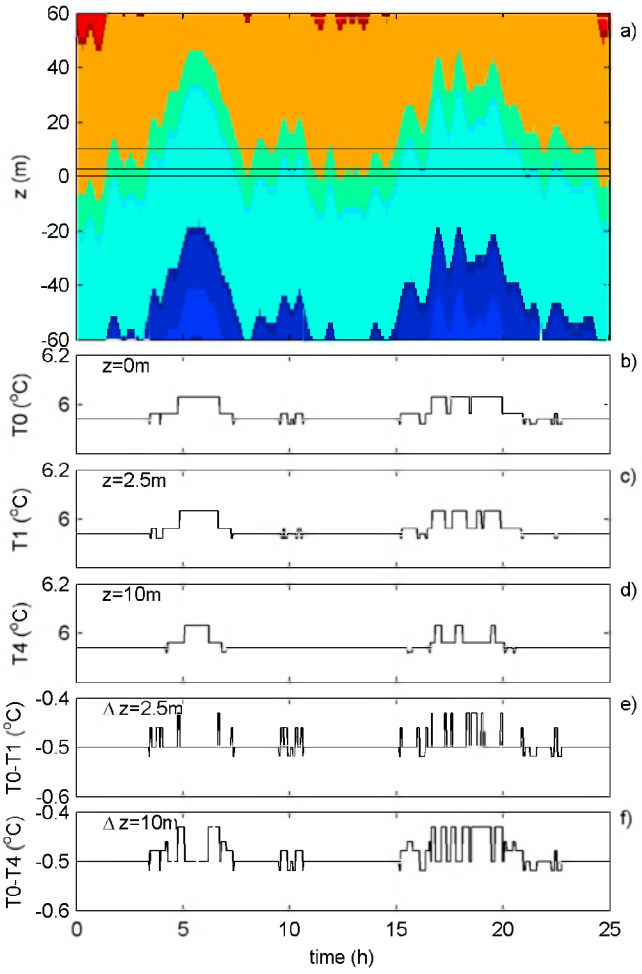

Figure 5. Synthetic temperature data produced by the advection of the temperature profile in Figure 4 by the filtered elevation signal ζ^*. (a) Example one day of data with temperature gray scale ranges between 5.8 and 6.1°C. Horizontal lines correspond to the sensors located at (b) $z = 0$, (c) $z = 2.5$, and (d) $z = 10$ m, for which time series of temperature. The temperature difference between sensors located at (e) $z = 2.5$ and (f) $z = 10$ m and the sensor located at $z = 0$.

variance of the signal at these frequencies will not be representative of the signal amplitude, as it would be the case for a deterministic signal (for instance the M_2 semidiurnal lunar tide). To quantify motions in the near-N band, we define two limit frequencies σ_- and σ_+ in order to have 50% of the near-N band energy in the $\sigma_- - \sigma_+$ domain. This band is centered at $\sigma_m = 20$ cpd, the frequency at which the vertical velocity spectrum is (locally) maximal. This frequency slightly differs from $N = 26$ cpd. We filter the elevation signal using a band-pass filter between σ_- and σ_+ and compute the standard deviation of this signal $\zeta_m = 3.5$ m; we define $\bar{w} = 2\pi\sigma\zeta_m$ for σ in the band $\sigma_- - \sigma_+$ and deduce that the typical duration of the spikes present in the difference between two successive sensors is $\Delta t = \Delta z/2\pi\sigma\zeta_m$. When σ varies from σ_- to σ_+, the corresponding π-phase frequencies of the order of $1/\Delta t$ vary from $\sigma'_- = 2\pi\sigma_-\zeta_m/\Delta z$ to $\sigma'_+ = 2\pi\sigma_+\zeta_m/\Delta z$, and is centered at $\sigma'_m = 2\pi\sigma_m\zeta_m/\Delta z$. The advection of thin temperature steps thus transfers the near-N band into the π-phase band.

[22] The theoretical predictions for the π-phase band are in very good agreement both with the artificial data (Figure 6) and the observations (Figure 3). The shift of the π-phase band with Δz is correctly represented, and the width of the band also corresponds to the width of the near-N band in the vertical velocity spectrum. For $\Delta z > \zeta_m = 3.5$ m, the blockade at N_t is also represented, and results as expected from the predominance of zero-phase coherent motions in the internal wave bands. Fine-structure contamination is presumably also present at $\sigma < N_t$, but not statistically significant and thus impossible to measure. The fact that our kinematic model, which only generates local mode 1 motions, compares so well with the in situ data also indicates

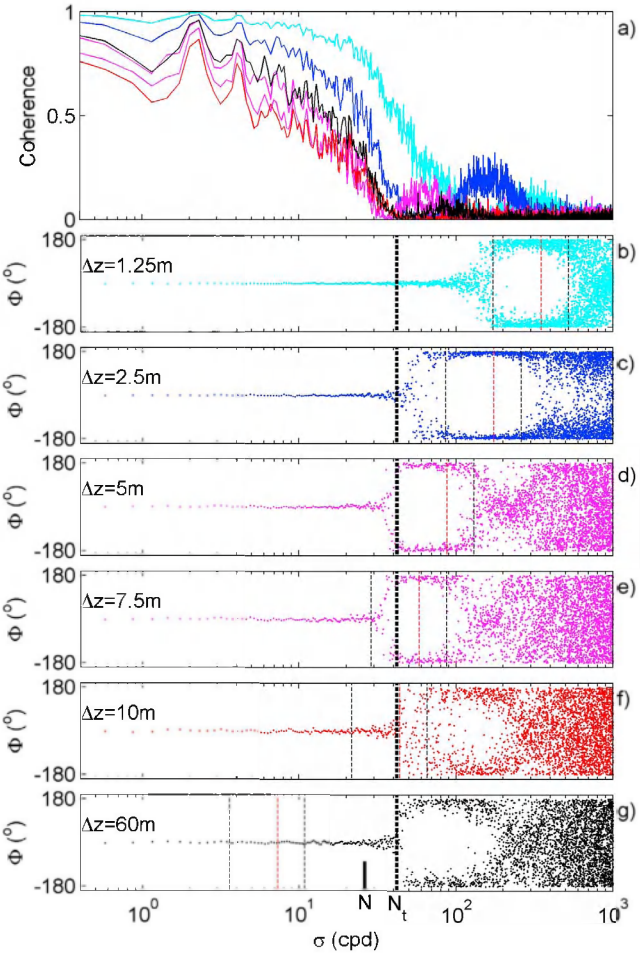

Figure 6. Artificial coherence spectra between virtual thermistors separated by Δz in the vertical. This computation uses the 200 day elevation signal of Figure 4a to advect the temperature profile of Figure 4b past the sensors. (a) The absolute value of coherence for $\Delta z = 1.25$ m (light blue line), 2.5 m (blue line), 5 m (magenta line), 7.5 m (magenta line), 10 m (red line), and 60 m (black line). (b–g) Phase with corresponding colors. The thick dashed line represents N_t, the transition frequency, whereas thin dashed black and red lines correspond to our theoretical model for the π-phase region.

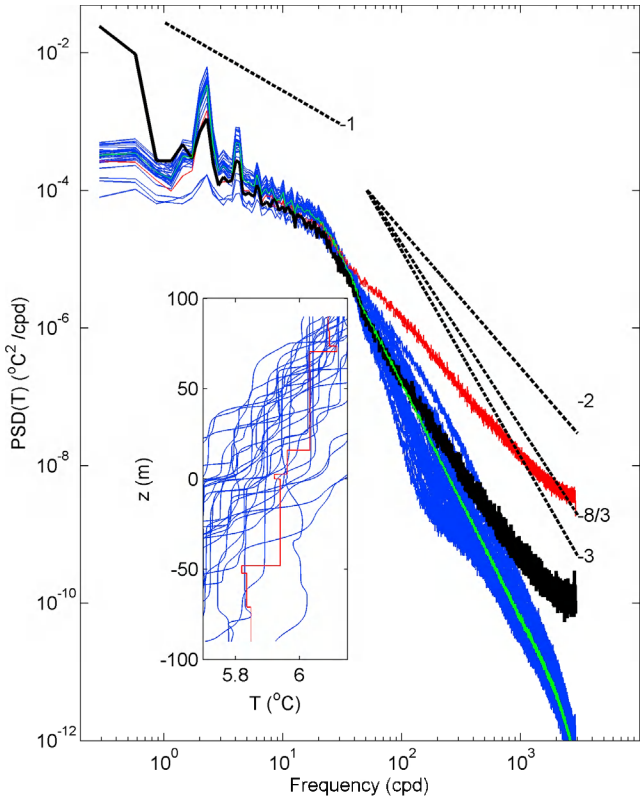

Figure 7. Temperature spectrum from in situ data (black) sloping as −8/3 in the 20–200 cpd frequency band. Spectrum using the kinematic model when the advected temperature profile has infinitely thin steps is shown in red; it slopes as −2. Spectra from the model using 30 different profiles with density jumps of finite thickness is shown in blue (see text for a statistical description of the profiles). The average of the 30 profiles is shown in green, sloping as −3. The profiles used are plotted in the inset (temperature between 5.7 and 6.15°C; same vertical scale as Figure 4).

that the pi-phase coherence cannot be attributed to local mode 2 or higher internal waves.

[23] Some π-phase region is still visible in our kinematic model at $\sigma > N_t$ for $\Delta z = 10$ m and 60 m. This is attributed to the periodicity of the steps in the artificial temperature profile. Two sensors separated by a vertical distance $\Delta z > \zeta_m = 3.5$ m will not be able to record the passage of the same temperature step. However, two successive steps, respectively in front of each sensor when the fluid is at rest, may also contribute to π-phase coherence. We have observed that steps of equal thickness in the temperature profile produce a Δz periodicity of their π-phase pattern, but the π-phase regions at Δz smaller than the vertical amplitude of the waves can already be observed with a single temperature step.

[24] In our model, the temperature profile is constant with time, whereas real temperature profiles at the mooring location slowly evolve with time, due to mixing and/or horizontal advection. As a result, the absolute value of coherence is higher in our model than in the ocean. This variability presumably affects the coherence phase for $\Delta z > \zeta_N$, and produces the random distribution of phase after the blockade seen in Figures 3f and 3g.

[25] We completely resolved the fine-structure contamination sketch, as predicted by *Phillips* [1971]. But more importantly, these results show that fine-structure contamination dominates the superbuoyant temperature signal in this specific data set. The π-phase regions would not be visible if any other phenomena, such as superbuoyant (nonlinear) waves or turbulence were affecting the temperature signal. This means that conclusions inferred from temperature spectra above N should be taken with care in the presence of steps in the temperature profile.

5. Discussion

[26] The direct coupling between high-frequency internal waves near the buoyancy frequency and superbuoyant motions traditionally relates to an important process for diapycnal mixing. This is because the latter are associated with the largest turbulent overturns, especially when they form closed contours and thus transport material, in stark contrast with linear waves. So far, the present coupling between internal wave band and turbulent scales outside it has not been observed in the ocean. In the present data set, however, we show that fine-structure contamination is dominating the temperature signal at high frequencies, and that turbulent processes above N may be non detectable. The data set acquired in the Madeira-Canary Basin should have a sufficient spatial and temporal resolution to resolve turbulence in the weakly stratified layers. It appears that kinematic effects, namely vertical advection of steps in the temperature profile, create strong π-phase coherence, which is visible only in the superbuoyant region. The standard deviation ζ^* of the elevation signal at $\sigma \simeq N$ governs, for a given Δz, the frequency range over which π-phase coherence is observed.

[27] As an illustration, we reproduce in Figure 7 the spectrum of the temperature signal measured by one single thermistor (black line), and several temperature spectra obtained from our model. As stated in *van Haren and Gostiaux* [2009], the spectrum from the in situ data slopes like $\sigma^{-8/3}$. The presence of the π-phase regions for different Δz indicate that fine-structure contamination dominates the temperature signal in the superbuoyant part of the spectrum for the present data set. Fine-structure contamination is traditionally associated with a σ^{-2} slope, as predicted by *Phillips* [1971] in the case of infinitely thin steps in the temperature profile. When we use infinitely thin steps, as in the previous sections of the present article, this σ^{-2} slope is observed (Figure 7, red line). We also produced 30 different temperature profiles with steps of nonzero thickness. The statistical properties for the number of steps, the vertical position of the steps and the steps amplitude was identical as in section 4, but the temperature jump of each step was no longer described by the Heaviside function $H(z)$ as in equation (1). Instead, the function $\tanh(z/\delta_k)$ was used, δ_k being uniformly random between 0.25 and 4.75 m. The π-phase behavior remains the same, as well as their frequency range (only depending on Δz and ζ_N, not shown), but the spectral slope above N can take values different from σ^{-2} (Figure 7, blue line). The average spectrum using the 30 independent realizations slopes like −3. The canonical σ^{-2} slope for infinitely sharp steps appears to be only a limiting

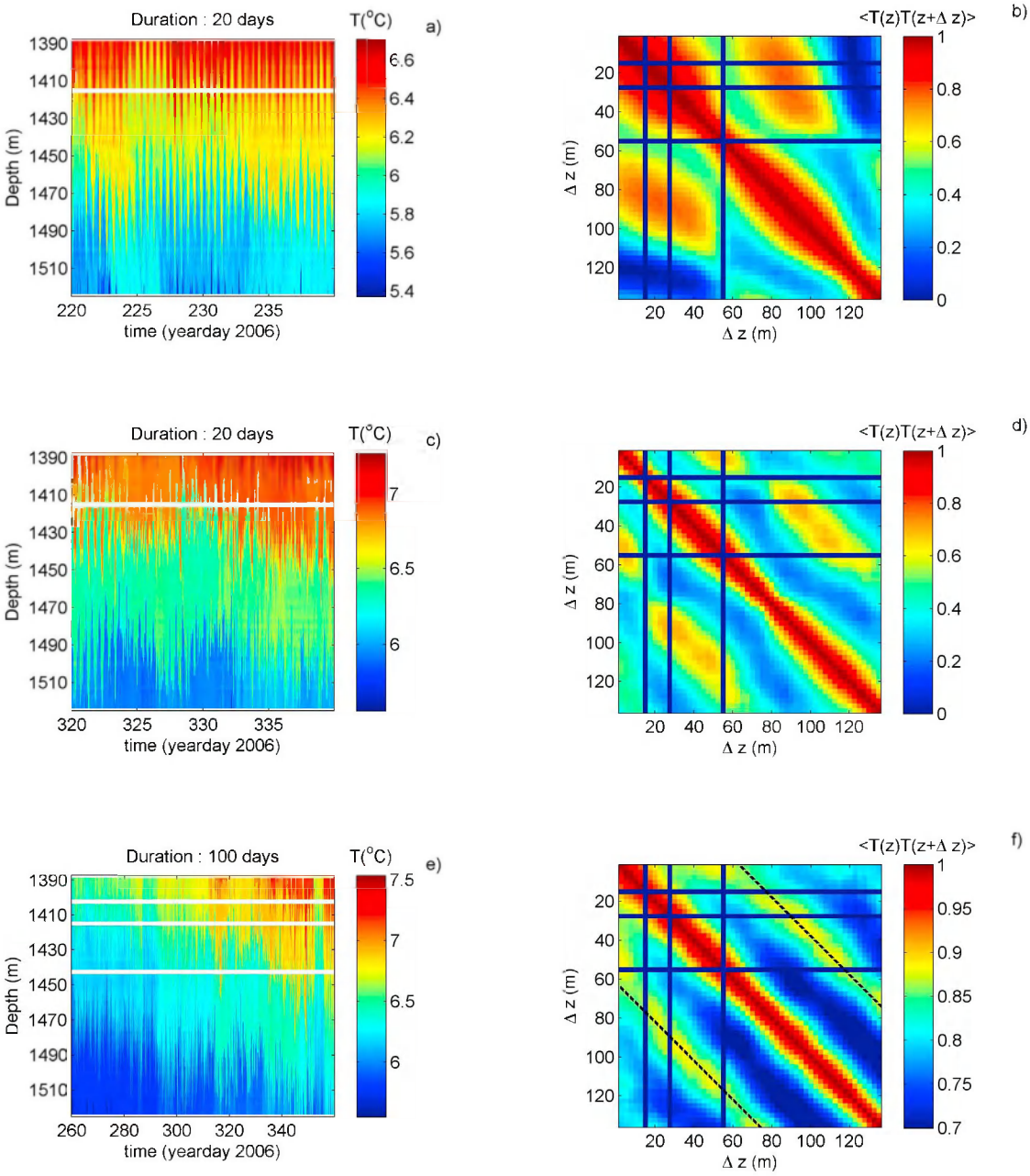

Figure A1. Cross correlations between the 53 NIOZ HST thermistors. (a and c) The temperature for two different 20 day periods. (b and d) The corresponding cross-correlation patterns. (e and f) Plots computed using a 100 day period, indicating an increase of coherence for $\Delta z = 62$ m, which is the typical value of the homogeneous layers thickness. Note the different color bar in Figure A1f.

case for fine-structure contamination in the ocean, and further theoretical developments are needed to understand how spectral slopes different from -2 can be obtained.

[28] Another ingredient of fine-structure contamination in the ocean is the variation of the temperature profile at large time scales; our kinematic model uses a single profile to successfully produce the π-phase regions in the frequency range; the location of the π-phase region is independent of the precise shape of the profile. However, in situ data show variations of the temperature profile over a time scale O (10 days). Monthly variability of the temperature spectrum tail was also observed [see *van Haren and Gostiaux*, 2009, Figure 11] and is probably related to changes in the temperature profiles. The nature of these changes, presumably horizontal advection of sloping isotherms, is under investigation.

Appendix A: Cross Coherence of Vertically Separated Temperature Signals Used to Estimate Typical Layers Thickness

[29] The coherence spectra using in situ data in Figure 3 show the evolution of the correlation between two sensors in the frequency domain. The correlation between two temperature signals over the entire period would be the integral

of the coherence spectrum over the frequency domain. This cross correlation between sensors is easy to compute and to display as a function of sensor spacing. Two different periods of 20 days were used to compute the cross correlation from the in situ temperature data (Figures A1a and A1b). The pattern is symmetrical, and correlation has the highest value along the diagonal and decreases as the distance between the sensors increases (Figures A1c and A1d); such a decrease was described by *Cairns and Williams* [1976], but surprisingly, high values of correlation up to 0.7 are reached for larger distances between the sensors. The precise location of these correlation patches vary in time, related to the respective depths of successive temperature jumps; when the cross correlation is computed over larger periods of time (Figure A1c, 100 days), the patches average over a sharp band corresponding to $\bar{D} = 60$ m. This distance is interpreted as the characteristic thickness of homogeneous temperature layers in the present data set.

[30] **Acknowledgments.** We thank the crew of the RV *Pelagia* for deployment and recovery of our moorings. We enjoyed discussions with Martin Laan on all aspects of NIOZ's thermistor strings. The construction and deployment of NIOZ3 were financed by investment grants ("Oceanographic equipment" and "LOCO," respectively) from the Netherlands organization for the advancement of scientific research, NWO. L.G. was supported in part by BSIK and by ANR 2011 Blanc SIMI 5-6 012-03 (OLA).

References

Alford, M. H., and R. Pinkel (2000), Observations of overturning in the thermocline: The context of ocean mixing, *J. Phys. Oceanogr.*, *30*, 805–832.

Cairns, J., and G. Williams (1976), Internal wave observations from a midwater float: 2, *J. Geophys. Res.*, *81*, 1943–1950.

Ferrari, R., and C. Wunsch (2009), Ocean circulation kinetic energy: Reservoirs, sources, and sinks, *Annu. Rev. Fluid Mech.*, *41*, 253–282.

Fu, L.-L., T. Keffer, P. Niiler, and C. Wunsch (1982), Observations of mesoscale variability in the western North Atlantic: A comparative study, *J. Mar. Res.*, *40*, 809–848.

Gargett, A. E., P. J. Hendricks, T. B. Sanford, T. R. Osborn, and A. J. Williams (1981), A composite spectrum of vertical shear in the upper ocean, *J. Phys. Oceanogr.*, *11*, 1258–1271.

Garrett, C. (1990), The role of secondary circulation in boundary mixing, *J. Geophys. Res.*, *95*, 3181–3188.

Garrett, C., and W. Munk (1971), Internal wave spectra in the presence of fine structure, *J. Phys. Oceanogr.*, *1*, 196–202.

Garrett, C., and W. Munk (1972), Space-time scales of internal waves, *Geophys. Fluid Dyn.*, *54*, 225–264.

Gregg, M. (1977), Variations in the intensity of small-scale mixing in the main thermocline, *J. Phys. Oceanogr.*, *7*, 436–454.

Gregg, M. C., and C. S. Cox (1972), The vertical microstructure of temperature and salinity, *Deep Sea Res.*, *19*, 355–376.

Joyce, T. M., and Y. J. F. Desaubies (1977), Discrimination between internal waves and temperature fine structure, *J. Phys. Oceanogr.*, *7*, 22–32, doi:10.1175/1520-0485(1977)007<0022:DBIWAT>2.0.CO;2.

Magnell, B. (1976), Salt fingers observed in the Mediterranean outflow region (34°N, 11°W) using a towed sensor, *J. Phys. Oceanogr.*, *6*(4), 511–523.

McKean, R. S. (1974), Interpretation of internal wave measurements in the presence of fine-structure, *J. Phys. Oceanogr.*, *4*, 200–213.

Merryfield, W. J. (2000), Origin of thermohaline staircases, *J. Phys. Oceanogr.*, *30*(5), 1046–1068.

Munk, W. (1966), Abyssal recipes, *Deep Sea Res.*, *13*, 707–730.

Munk, W., and C. Wunsch (1998), Abyssal recipes II: Energetics of tidal and wind mixing, *Deep Sea Res.*, *45*, 1977–2010.

Osborn, T. R., and C. S. Cox (1972), Oceanic fine structure, *Geophys. Fluid Dyn.*, *3*, 321–345.

Phillips, O. M. (1971), On spectra measured in an undulating layered medium, *J. Phys. Oceanogr.*, *1*, 1–6.

Phillips, O. M. (1977), *The Dynamics of the Upper Ocean*, Cambridge Univ. Press, Cambridge, U. K.

Pinkel, R. (1981), Observations of the near-surface internal wavefield, *J. Phys. Oceanogr.*, *11*, 1248–1257.

Pinkel, R., A. Pluedemann, and R. Williams (1987), Internal wave observations from flip in MILDEX, *J. Phys. Oceanogr.*, *17*, 1737–1757.

Thorpe, S. (2010), Breaking internal waves and turbulent dissipation, *J. Mar. Res.*, *68*, 851–880.

van Haren, H., and L. Gostiaux (2009), High-resolution open-ocean temperature spectra, *J. Geophys. Res.*, *114*, C05005, doi:10.1029/2008JC004967.

van Haren, H., and L. Gostiaux (2010), A deep-ocean Kelvin-Helmholtz billow train, *Geophys. Res. Lett.*, *37*, L03605, doi:10.1029/2009GL041890.

van Haren, H., M. Laan, D.-J. Buijsman, L. Gostiaux, M. G. Smit, and E. Keijzer (2009), NIOZ3: Independent temperature sensors sampling yearlong data at a rate of 1 Hz, *IEEE J. Oceanic Eng.*, *34*, 315–322.